https://doi.org/10.1016/j.cjche.2019.06.004

Parametric Optimization of Packed Bed for Activated Coal Fly Ash Waste Heat Recovery Using CFD Techniques

Kai Liang[a], Saimeng Jin[a], Hengzhi Chen[a], Weifeng Shen[*,a], Jingzheng Ren[b] and Shun'an Wei[*,a]

[a]School of Chemistry and Chemical Engineering, Chongqing University, Chongqing 400044, China

[b]Department of Industrial and Systems Engineering, The Hong Kong Polytechnic University, Hong Kong SAR, China

Corresponding Author:*E-mail: (W.S) shenweifeng@cqu.edu.cn;(S.W) wsacn@cqu.edu.cn

Abstract: Coal fly ash is an industrial solid waste generated from coal preparation during the processing and cleaning of coal for electric power generation. Comprehensive investigation on the reutilization of waste heat of activated coal fly ash is of great economic significance. The method of recovering the waste heat, proposed in this study, is the transfer of heat from activated coal fly ash to gas with the movement of air using the packed bed, providing valuable energy sources for preheating the raw coal fly ash to reduce the overall energy consumption. The investigation is carried on the heat transfer characteristics of gas-solid (activated coal fly ash) phases and air temperature fields of the packed bed under some key conditions *via* computational fluid dynamics. A two dimensional geometry is utilized to represent key parts of packed bed. The distribution mechanism of the temperature field for gas phase is analyzed based on the transient temperature contours at different times. The results show that the obtained rule of gas-solid heat transfer can effectively evaluate the influences of operating parameters on the air temperature in the packed bed. Simultaneously, it is found that no temperature differences exist in the hot air at the outlet of the packed bed. The investigation provides guidance for the design and optimization of other similar energy

recovery apparatuses in industries.

Keywords: Coal fly ash; Computational fluid dynamics; Eulerian-Eulerian model; Waste heat recovery; Packed bed

1. Introduction

With the development of industrial communities and ever-increasing demand for energy, the consumption of fossil fuels has increased significantly, which intensifies the concerns associated with limited nature of the sources of such energy [1]. Statistics suggested that the equivalent coal consumption of China had been 3.75 billion tons in 2013, accounting for more than half of global consumption [2]. Meanwhile, the traditional chemical industry with the characteristics of high energy consumption is full of waste heat resources that account for about 17%-67% of the total heat energy of the fuels. For the past few years, with the increase in the demand for energy and also concerns about climate changes, it is widely believed that energy recovery is an effective measure to reduce energy consumption [3]. Generally, the waste heat resources can be divided into three categories including gas [4], liquid [5] and solid particles [6-8]. Among them, the heat utilization of gas and liquid with high temperature has been widely studied while the corresponding technology is relatively mature. However, one challenge will be how to utilize the waste heat of solid particles with high temperature nowadays.

Coal fly ash (CFA), a by-product generated by the high temperature combustion of coal in coal-fired power plants, contains more than 90% of SiO_2, Al_2O_3 and carbon-based components, which can be exploited as an important resource for extracting aluminum and silicon [9, 10]. The raw CFA has relatively lower dissolution rate at normal temperature in virtue of stable structure [11]. It has been found that calcination can promote the reactivity of CFA to enhance alumina extraction [12] by transferring Al_2O_3 into γ-Al_2O_3 [13]. When activated CFA is discharged from calciner at a high temperature of 850℃, it takes abundant heat away from the calcination process. It should be emphasized that the calcination of the raw CFA at 1123 K makes agglomeration of smaller particles feasible [14]. At present, about 800 million tons of the activated CFA is produced by the calcination annually in the world. If the waste heat is recovered completely, this will save 32 million tons of standard coal equivalently. However, the improvement of the conventional process for waste heat recovery of activated CFA with high energy has become increasingly imminent and needs to be implemented.

Recently, several researchers have focused on the waste heat reutilization of the steel slag. Cai *et al*. [15] and Ding *et al*. [16] summarized the current energy structure of steel industry and the distribution of waste heat for steel production. Chen *et al*. [17] analyzed the flow-field and temperature-field of steel slag and studied the temperature change of air at outlet when the flow velocity at inlet were varied. The effects of operational parameters, moving speed of material layer and depth of buried material on heat transfer coefficient were also studied. The movement of irregularly arranged particle near the wall had been simulated with CFD [18]. The axial heat transfer characteristics in packed bed and the heat transfer coefficient of vertical pipes had been reported [19]. Although these studies mainly conclude the heat transfer characteristics of gas-solid phases in the production of steel slag, they can be used as a reference to study the waste heat recovery of activated CFA. However, the physical properties of the activated CFA distinguishing from the steel slag may affect heat transfer characteristics of gas-solid phases. As such, the exploration of the waste heat reutilization of activated CFA plays an important role in the design and optimization of energy recovery apparatuses.

Motivated by the preceding researches, in this contribution, we focus on developing a method of recovering the waste heat by transferring the heat from activated CFA to gas with the movement of air using the packed bed. A theoretical transient model with CFD is utilized to describe the heat transfer characteristics of gas-solid direct contact and air temperature fields in the packed bed. Afterwards, the finite volume method using the 'phase couple SIMPLE' algorithm to handle pressure-velocity and phase coupling is applied to solve the heat transfer problem. It should be noted that this analysis of heat transfer characteristics is made mainly in terms of outlet air temperature. Accordingly, the heat transfer characteristics of gas-solid can be obtained without pilot test. Then, the novelty of the proposed method is that the rich heat resource of activated CFA is reutilized to provide valuable energy sources for preheating the raw CFA achieving the reduction of the overall energy consumption. To clarify the important sense of the proposed method, a detailed description is presented with case evaluation of four key operating parameters. In this sense, the contribution of this study is to provide guidance for the design and optimization of demonstration apparatuses in the process of activated CFA waste heat recovery.

2. Process description

In the CFA activation, the raw CFA is preheated firstly and then calcined at 1123 K. Subsequently, the outlet of the calciner is discharged into a packed bed, and it is cooled to the room temperature by air to acid leacher for extract aluminum. Following that, the generated hot air is utilized to preheat the raw CFA for decreasing the heat duty of the calciner. The investigations on solid calcination and gas-solid separation in the CFA activation are extensively studied. A special-type cyclone that has double conical sections is employed to collect fine particles under high temperature [20]. García *et al*. [21] proposed a new sintering model to account for the contribution of high calcination temperatures and times to solid sintering. However, few studies have been focused on the explorations on waste heat utilization of activated CFA. As such, we focus on developing a method of recovering the waste heat using the packed bed to reduce the overall energy consumption in the CFA activation. The flow sheet of the CFA activation is described in Fig. 1.

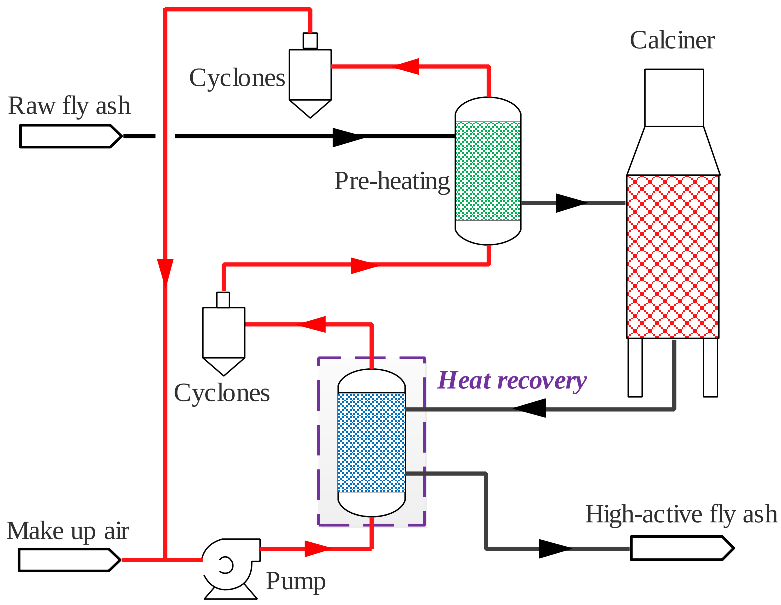

Fig. 1 The flow sheet of the CFA activation

The packed bed is one of most important reactors, which has been widely used in the chemical industries such as the trickled bed [22], coal gasification [23] and heat exchangers [24, 25]. It is critical to evaluate gas-solid direct-contact heat transfer in packed bed for determining the safe operating condition and optimizing the relevant devices [26, 27]. In fact, many factors are proposed to predict gas-solid direct contact heat transfer including the particle diameter, the local fluid velocity, solid packing height and the solid volume fraction. Thus, most equations for representing gas-solid direct contact heat transfer are semi-empirical and obtained by fitting the experimental data of air temperature. To improve the accuracy, the crucial factors of gas-solid heat transfer characteristic are studied as many as possible by correlating the relevant parameters [28]. However, the calculating results are not significantly improved by incorporating more influencing factors into the relevant semi-empirical equations. As far as we known, a general acceptable method has not yet been developed. As a result, the expensive pilot plants for commercializing a process of waste heat recovery in packed bed has not been well built to determine optimum and safe operating conditions. This work presents a study undertaken on modeling gas-solid direct contact heat transfer based on the Euler description of the phases and multiphase fluid-dynamic model to provide a theoretical guidance to real industry process.

3. Mathematical model

3.1 Model selection

Generally, gas-solid flow can be modeled at particle scales and macro levels by local averaging based on the application and required information. The particle scale approach tracks the motion of individual particles using a discrete element method (DEM), and the flow of air using a continuum based CFD model with local properties averaged over a number of computational cells. The multiphase flow model is commonly referred to as a DEM-CFD model [29, 30]. The macro level approach treats both solid and gas phase as interpenetrating continua and the motion of each phase is solved using a continuum based CFD model with suitable closure terms. This method is known as Euler-Euler model [31]. DEM-CFD models can predict detailed solid flow behavior with the disadvantage of computationally demanding [32]. The EEMs take less computational time, however, the accuracy relies on the closure model employed to describe properties such as solid viscosity and solid pressure. Both models are widely utilized to explore various gas-solid flow behaviors and are areas of ongoing research at CSIRO [33]. Finally, the Eulerian-Eulerian model is employed to analyze gas-solid flows in a packed bed. The gas phase flow is assumed to be steady, incompressible and fully developed. The flow field of gas phase is simulated by the standard *k*-*ε* turbulence model [34] to deal with the interphase turbulent momentum transfer.

3.2 Euler-Euler model and *k*-*ε* turbulence model equations

A summary of the governing equations along with the associated constitutive sub-models of the Euler-Euler (E-E) model and *k*-*ε* turbulence model is presented in this section. These equations describe conservation of mass and momentum for each phase [35] as well as the conservation of fluctuating translational kinetic of the solid phase based on the kinetic theory of granular flow.

Air and CFA mass conservation equations:

$$\frac{\partial(\alpha_a \rho_a)}{\partial t} + \nabla(\alpha_a \rho_a \boldsymbol{u}_a) = 0 \tag{1}$$

$$\frac{\partial(\alpha_s \rho_s)}{\partial t} + \nabla(\alpha_s \rho_s \boldsymbol{u}_s) = 0 \tag{2}$$

Where α_α represents the air volume fraction, α_s is the solid volume fraction, ρ_α refers to the air density, ρ_s is the solid density, $\boldsymbol{u}_\alpha$ represents air velocity vector, $\boldsymbol{u}_s$ refers to solid velocity vector.

Air and CFA momentum conservation equations:

$$\frac{\partial(\alpha_a\rho_a\boldsymbol{u}_a)}{\partial t}+\nabla\left[\alpha_a\rho_a\boldsymbol{u}_a\cdot\boldsymbol{u}_a-\alpha_a\mu_a\left\{\nabla\boldsymbol{u}_a+(\nabla\boldsymbol{u}_a)^T\right\}\right]=-\alpha_a\nabla p+\beta(\boldsymbol{u}_s-\boldsymbol{u}_a)+\alpha_a\rho_a\boldsymbol{g} \tag{3}$$

$$\frac{\partial(\alpha_s\rho_s\boldsymbol{u}_s)}{\partial t}+\nabla\left[\alpha_s\rho_s\boldsymbol{u}_s\cdot\boldsymbol{u}_s\right]=-\alpha_s\nabla p+\beta(\boldsymbol{u}_a-\boldsymbol{u}_s)+\alpha_s\rho_s\boldsymbol{g}+\nabla\sigma_s \tag{4}$$

$$\sigma_s=\left[-P_s+\xi_s\nabla\boldsymbol{u}_s\right]\boldsymbol{I}+2\mu_s\boldsymbol{S}_s \tag{5}$$

$$\xi_s=\frac{4}{3}\alpha_s{}^2\rho_s\mathrm{d}_p g_0(1+e)\sqrt{\theta/\pi} \tag{6}$$

$$\boldsymbol{S}_s=\frac{1}{2}\left[\nabla\boldsymbol{u}_s+(\nabla\boldsymbol{u}_s)^T-\frac{1}{3}\nabla\boldsymbol{u}_s\boldsymbol{I}\right] \tag{7}$$

Where β is interphase momentum transfer coefficient, d_p represents particle diameter, e refers to coefficient of restitution, $\boldsymbol{g}$ is gravity vector, g_0 represents radial distribution function, $\boldsymbol{I}$ refers to identity tensor, P_s is pressure of fly ash, σ_s represents solid stress tensor, ζ_s refers to fly ash bulk viscosity, θ is granular temperature, μ_α represents air viscosity, μ_s is fly ash viscosity.

CFA kinetic energy conservation equation:

$$\frac{3}{2}\left[\frac{\partial(\alpha_s\rho_s\theta)}{\partial t}+\nabla(\alpha_s\rho_s\boldsymbol{u}_s\theta)\right]=\sigma_s:\nabla\boldsymbol{u}_s-\nabla(-\kappa_s\nabla\theta)-\gamma \tag{8}$$

Where κ_s represents fly ash thermal conductivity, γ refers to collisional dissipation of solid fluctuating kinetic energy.

CFA shear viscosity:

$$\mu_s=\mu_{s,collision}+\mu_{s,kinetic}+\mu_{s,frictional} \tag{9}$$

$$\mu_{s,collision}=\frac{4}{5}\alpha_s{}^2\rho_s d_p g_o(1+e)\sqrt{\theta/\pi} \tag{10}$$

$$\mu_{s,kinetic}=\frac{\alpha_s\rho_s d_p(\theta\pi)^{\frac{1}{2}}}{6(3-e)}\left[1+\frac{2}{5}(1+e)(3e-1)\alpha_s g_o\right]$$

(11)

$$\mu_{s,frictional}=\frac{P_{s,frictional}\sin\phi}{2\sqrt{I_{2D}}} \tag{12}$$

Where I_{2D} is second invariant of deviatoric stress tensor, ϕ refers to internal friction angle.

CFA pressure:

$$p_s = p_{s,kinetic} + p_{s,frictional} \tag{13}$$

$$p_{s,kinetic} = \rho_s \alpha_s \theta \left[1 + 2(1{+}\mathrm{e})\alpha_s g_0\right] \tag{14}$$

$$p_{s,frictional} = \begin{cases} 10^{25}\left(\alpha_s - \alpha_{s,\max}\right)^{10} & \alpha_s > \alpha_{s,\max} \\ 0 & \alpha_s \le \alpha_{s,\max} \end{cases} \tag{15}$$

Where $\alpha_{s,max}$ represents maximum solid volume fraction.

Diffusivity of CFA temperature:

$$\kappa_s = \frac{150\rho_s d_p \sqrt{\pi\theta}}{384(1+e)g_0}\left[1 + \frac{6}{5}\alpha_s g_0 (1+e)\right]^2 + 2\alpha_s{}^2 \rho_s d_p g_0 (1+e)(\frac{\theta}{\pi})^{1/2} \tag{16}$$

Collision energy dissipation:

$$\gamma = \frac{12(1-e^2)\rho_s g_0}{d_p\sqrt{\pi}}\alpha_s{}^2\sqrt{\theta^3} \tag{17}$$

$$g_0 = \left[1 - \sqrt[3]{\frac{\alpha_s}{\alpha_{s,\max}}}\right]^{-1} \tag{18}$$

The drag force [36] is the only accelerating force acting on particles playing an important role in gas-solid two-phase flows. The Gidaspow drag [37] model give the best agreement with a dense packed bed. Generally, the drag force acting on particles in gas-solid system can be represented by the product of a momentum transfer coefficient β and the slip velocity ($\boldsymbol{u}_s$-$\boldsymbol{u}_\alpha$) between the two phases:

$$\beta = 150\frac{\alpha_s{}^2\mu_a}{\alpha_a d_p{}^2} + 1.75\frac{\alpha_s\rho_a}{d_p}\left|\boldsymbol{u}_s - \boldsymbol{u}_a\right| \quad \alpha_a < 0.8 \tag{19}$$

$$\beta = \frac{3}{4} C_D \frac{\alpha_a \alpha_s \rho_a}{d_p} \left| \boldsymbol{u}_s - \boldsymbol{u}_a \right| \alpha_a^{-2.65} \qquad \alpha_a \geq 0.8 \tag{20}$$

Where the drag coefficient C_D is expressed by

$$C_D = \begin{cases} \frac{24}{\alpha_a R_{ep}} \left[1 + 0.15 (\alpha_a R_{ep})^{0.687} \right] & R_{ep} < 1000 \\ 0.44 & R_{ep} \geq 1000 \end{cases} \tag{21}$$

$$\mathrm{Re}_p = \frac{\rho_a d_p \left| \boldsymbol{u}_s - \boldsymbol{u}_a \right|}{\mu_a} \tag{22}$$

Where, Re_p is Reynolds number of CFA.

Turbulence k-ε model is used to evaluate the turbulent kinetic energy k and turbulent energy dissipation rate ε, respectively.

$$\frac{\partial(\alpha_\alpha \rho_\alpha k_\alpha)}{\partial t} + \nabla \cdot (\alpha_\alpha \rho_\alpha \boldsymbol{u}_\alpha k_\alpha) = \nabla \cdot \left(\alpha_\alpha \frac{\mu_{t,\alpha}}{h_k} k_\alpha \right) + \alpha_\alpha G_{k,\alpha} - \alpha_\alpha \rho_\alpha \varepsilon_\alpha + \alpha_\alpha \rho_\alpha \Pi_{k,\alpha} \tag{23}$$

$$\frac{\partial(\alpha_\alpha \rho_\alpha \varepsilon_\alpha)}{\partial t} + \nabla \cdot (\alpha_\alpha \rho_\alpha \boldsymbol{u}_\alpha \varepsilon_\alpha) = \nabla \cdot \left(\alpha_\alpha \frac{\mu_{t,\alpha}}{h_\varepsilon} \varepsilon_\alpha \right) + \alpha_\alpha \frac{\varepsilon_\alpha}{k_\alpha} \left(C_1 G_{k,\alpha} - C_2 \rho_\alpha \varepsilon_\alpha \right) + \alpha_\alpha \rho_\alpha \Pi_{\varepsilon,\alpha} \tag{24}$$

Where k_α represents turbulence kinetic energy of gas phase, ε_α is turbulent energy dissipation rate of gas phase, $\mu_{t,\alpha}$ refers to gas phase turbulent viscosity, $G_{k,\alpha}$ is rate of production of turbulent kinetic energy, $\Pi_{k,\alpha}$ represents turbulent interaction parameters, h_k is interfacial tension of turbulence kinetic energy, h_ε refers to interfacial tension of turbulent energy dissipation rate.

3.3 Heat transfer in solid packed bed

The heat transfer rates is significantly improved as a result of a large contact area between solid particles and the fluidizing air in the packed bed [38]. The enhancement of heat transfer resulting from air disturbance decreases the appearance of temperature gradients through the bulk of the bed and gives rise to a high internal thermal conductivity. In this sense, the understanding of the heat transfer mechanisms is crucial for an optimal process design. Furthermore, three heat transfer mechanisms are utilized to describe the heat transport phenomena involving fluid-particle convection, particle-particle conduction and particle radiation in the packed bed. According to Green et al. [39], symmetrical diatomic gases (such as O_2, N_2) are considered to be transparent bodies at high temperatures because they have neither the ability to radiate nor the ability to absorb. In this study, the air is selected as coolant and the main components of air are oxygen and nitrogen with symmetric molecular structures. The heat radiation between air and solid can be therefore neglected.

3.3.1 Mechanism of thermal conduction

The contacting thermal conductivity can be calculated from the thermal joint resistance including four thermal resistances [40-43]: (1) the macro-contact constriction/spreading resistance, R_L; (2) the micro-contact constriction/spreading resistance, R_S; (3) the resistance of interstitial air in the micro-gap, R_g; (4) the resistance of interstitial air in the macro-gap, R_G. R_g remains small for the four thermal resistances and can be neglected. Consequently, the joint resistance can be described by eq. (23).

$$R_j = \left[\frac{1}{R_S + R_L} + \frac{1}{R_G} \right]^{-1} \tag{23}$$

Where R_S is calculated as:

$$R_S = \frac{0.565 H^* (\sigma / m)}{\kappa_s F} \tag{24}$$

Where H^* is micro-hardness of particles; σ represents mean surface roughness height of particles; m refers to mean surface roughness slope of particles; K_S is the thermal conductivity of particles; F is the normal contact force. This force can be a result of the following factors including exerted external load on the packed bed, packing under pressure, thermal expansion of the particles and the structural load due to the weight of spheres, *etc*. In practice, the packed bed is a non-homogenous medium of different thermal conductivities corresponding to local variation of contact force. The contact load should be variable at different locations of packed bed. However, the thermal resistance is evaluated by considering an average contact force to simplify the calculating process.

Where F is the drag between the fluid and particles and it is approximately estimated according to the Ergun equation; H_{bed} represents the height of packed bed.

$$F = F_i \cdot H_{bed} \cdot \frac{\pi}{4} d_p^{\ 2} \tag{25}$$

$$F_i = \beta \cdot u_{\alpha i} \quad i = x, y \tag{26}$$

The macro-contact constriction/spreading resistance R_L can be expressed as:

$$R_L = \frac{1}{2\kappa_s r_L} \tag{27}$$

Where K_s is thermal conductivity coefficient of solids; r_L is the macro-contact radius.

$$\frac{\mathrm{r}_L}{r_H} = \begin{cases} \dfrac{1.605}{\sqrt{\psi}} & 0.01 \le \psi \le 0.47 \\ 3.51 - 2.51\psi & 0.47 \le \psi \le 1 \end{cases} \tag{28}$$

Where parameter ψ can be written as:

$$\psi = \frac{1}{1 + 1.22\eta\tau^{-0.16}} \tag{29}$$

$$\eta = \frac{\sigma d_p}{2r_H^{\ 2}} \tag{30}$$

$$\tau = \frac{E^{'}}{H^{*}} \sqrt{\frac{d_p}{2\sigma}} \tag{31}$$

Where, the Hertzian contact radius r_H can be calculated by eq. (32).

$$r_H = \left(\frac{0.75 F d_p}{2E^{'}} \right)^{\frac{1}{3}} \tag{32}$$

Where, the effective elastic modulus E' can be written as:

$$E^{'} = \frac{E}{2(1-\nu^2)} \tag{33}$$

Where, E is the Young's modulus, and ν is the Poisson's ratio.

The resistance of interstitial air in the macro-gap R_G is described by eq. (34).

$$R_G = \frac{2}{\pi \kappa_\alpha \left[S \ln\left(\frac{S}{S-B} \right) - B \right]} \tag{34}$$

In the Eq. (19), the relevant parameters are calculated as:

$$B = 2\sqrt{\frac{d_p^{\ 2}}{4} - r_L^{\ 2}}$$

(35)

$$S = d_p - 2\frac{r_L^{\ 2}}{d_p} + M \tag{36}$$

The air parameter M is defined as:

$$M = \left[\frac{2(2-\alpha_T)}{\alpha_T} \right] \left(\frac{2\Gamma}{1+\Gamma} \right) \frac{1}{P_r} \Lambda \qquad P_r = \frac{\mu_\alpha C_P}{\kappa_\alpha} \tag{37}$$

Where, γ is radio of air specific heats; Pr is the Prandtl number of air and α_T is defined by eq. (38).

$$\alpha_T = \exp\left[-0.57 \left(\frac{T_S - 273}{273} \right) \right] \left(\frac{1.4 M_\alpha}{6.8 + 1.4 M_\alpha} \right) + \frac{2.4 \mu_\alpha}{(1+\mu_\alpha)^2} \left\{ 1 - \exp\left[-0.57 \left(\frac{T_S - 273}{273} \right) \right] \right\} \tag{38}$$

Where, M_g is molar mass of air and the value of Λ can be found as:

$$\Lambda = \frac{P_0}{P_\alpha} \frac{T_\alpha}{T_0} \Lambda_0 \tag{39}$$

Where, P_g is the pressure of vapor phase. Here, P_0 is set to be 101.325 KPa, T_0=273.15 K,

Λ_0=64 nm. For SC packing, the effective thermal conductivity can be written as:

$$\kappa_{\mathrm{cond}} = \kappa_{sc} = \frac{1}{R_j d_p} \tag{40}$$

For FCC packing, the effective thermal conductivity is written by eq. (41).

$$\kappa_{\mathrm{cond}} = \kappa_{FCC} = \frac{2\sqrt{2}}{R_j d_p} \tag{41}$$

Therefore, the effective thermal conductivity can be considered as a composite of SC and FCC packing. The effective thermal conductivity due to conduction can be approximately written as:

$$\kappa_{eff} = \kappa_{FCC} + (\kappa_{sc} - \kappa_{FCC})\frac{\varepsilon - 0.26}{0.216} \tag{42}$$

3.3.2 Mechanism of convective heat transfer

In the packed bed, the convective heat transfer is the transfer of heat from activated CFA to air by the movement of gas. The equation for the rate of convective heat transfer between solid and air is written by eq. (43).

$$Q_{s\alpha} = hA(T_s - T_\alpha) \tag{43}$$

Where h is convective heat transfer coefficient and A is the total interfacial surface area of solid particles contact with air.

$$h = \frac{N_u k_\alpha}{d_p} \tag{44}$$

The Ranz-Marshall correlation [44] is utilized to describe the heat transfer coefficient characterizing convective heat transfer between air and the particles.

$$N_u = 2 + 0.6 R_e^{0.5} P_r^{0.3} \tag{45}$$

$$R_e = \frac{\alpha_s \rho_\alpha d_p \left|\boldsymbol{u}_\alpha - \boldsymbol{u}_s\right|}{\mu_\alpha} \tag{46}$$

4. Computational details

4.1 Geometry description

The waste heat recovery of activated CFA has been investigated *via* the application of packed bed. According to the mechanism of the interphase convective heat transfer, it is suggested that the activated CFA packed can preheat the cool air in the bed. Afterwards, the geometry of the packed bed in this study is based on the work of José Soria [45] with modification of the structure by amplify the bed as illustrated in Fig. 2. The two-dimensional (2D) packed bed has a length and width of 1000 mm and 400 mm, respectively. The model geometry includes a velocity inlet, wall and pressure outlet. The activated CFA is filled at the bottom of bed with different operation parameters including solid packing height, solid volume fraction, superficial air velocity, solid diameter to evaluate heat transfer characteristics of gas-solid phases. The characteristic of solid phase is determined by setting these values instead of by filling forms. The two-dimensional geometry of the bed is created to represent the actual case for proof-of-concept design and screening a large number of design options.

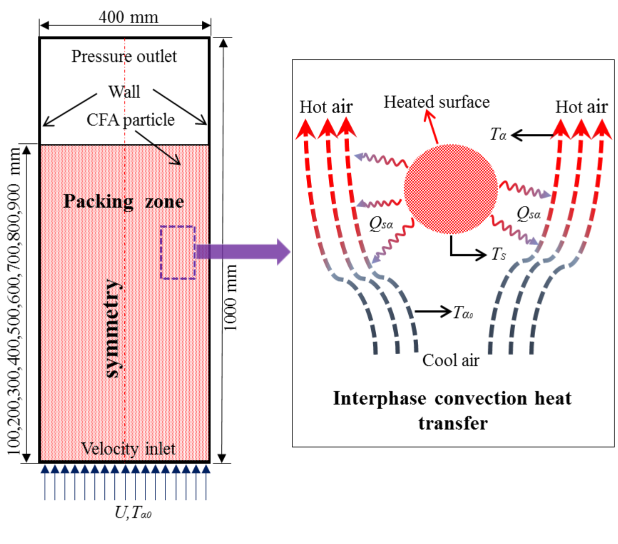

Fig. 2 Schematic diagram of the 2D packed bed geometry and interphase convection heat transfer

4.2 Model solution strategy

In the present investigation, the "phase couple SIMPLE" algorithm, which is an extension of the SIMPLE algorithm [46] to multiphase flows, is applied for the pressure-velocity. The multiphase flow model is proposed by Gidaspow *et al.* [47], which is widely utilized in packed bed study [48]. In addition, a second-order discretization scheme is used for convection terms in the momentum equations while the QUICK scheme is applied for the volume fraction equations. Afterwards, a time step of 0.01s with a second order implicit time integration scheme is utilized to advance the solution in time. It is utilized by Goldschmidt *et al.* to account for the loss of energy due to collision of particles in densely packed beds [49]. A decrease in the coefficient of restitution results in less elastic collision generating more fluctuating kinetic energy. Thus, the coefficient of restitution is possibly smaller in investigation cases. Besides, it is noteworthy that various researchers have further developed the EEM model including the use of a continuous stitching function to smoothly bridge the solid stresses from the viscous to the plastic regime in a spouting bed [50], modification of the drag law for size segregation study of binary systems [51], extension of kinetic theory to multiple particle sizes [52]. In recent years, DEM type of model has been used to build continuum process models for granular flow systems [53], however, this is still in an early stage for packed bed systems [54]. The simplified flow sheet of the simulation algorithm is also illustrated in Fig. 3.

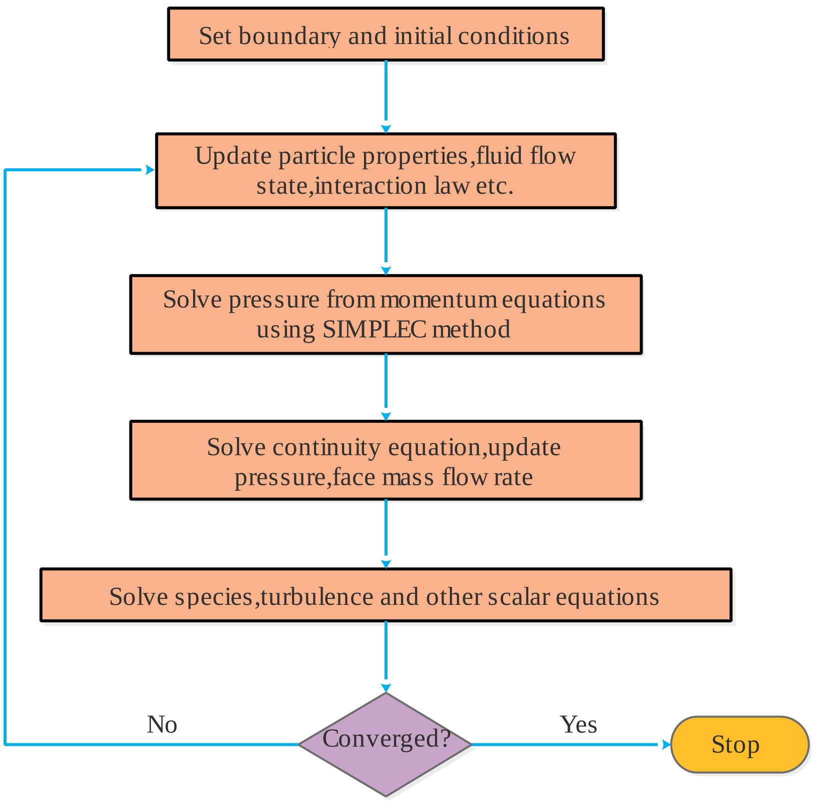

Fig. 3 Flow sheet of the calculation algorithm

4.3 Grid sensitivity study

It is important to construct the high quality meshes in the CFD modeling. The mesh density had been extensively investigated to determine the heat transfer characteristics of gas-solid phases of fixed bed in the early 1960s [55]. In order to guarantee the most suitable computational mesh grid and evaluate the effect of using different mesh size on the results, a grid independence study is carried out. The internal boundary is refined locally [56] when the bed model is meshed. Generally, the quantity and quality of the grid have a significant influence on the calculations. For obtaining the acceptable numerical solution, this work applies the structure grids produced from geometry models based on TTM method [57] to carry out grid-independence test. It is noted from Fig. 4 that there are three schemes for meshing and the quantity of grids are 400000, 4000 and 160, respectively. The calculations are carried under the conditions of relative velocity of 1 m/s, the solid diameter is 0.01 m, the initial solid packing height is 0.4 m and solid volume fraction is 0.63, respectively. When calculation is completed, the outlet air temperature is used as the evaluation standard. The comparison of the different grid quantity is presented in Table 1.

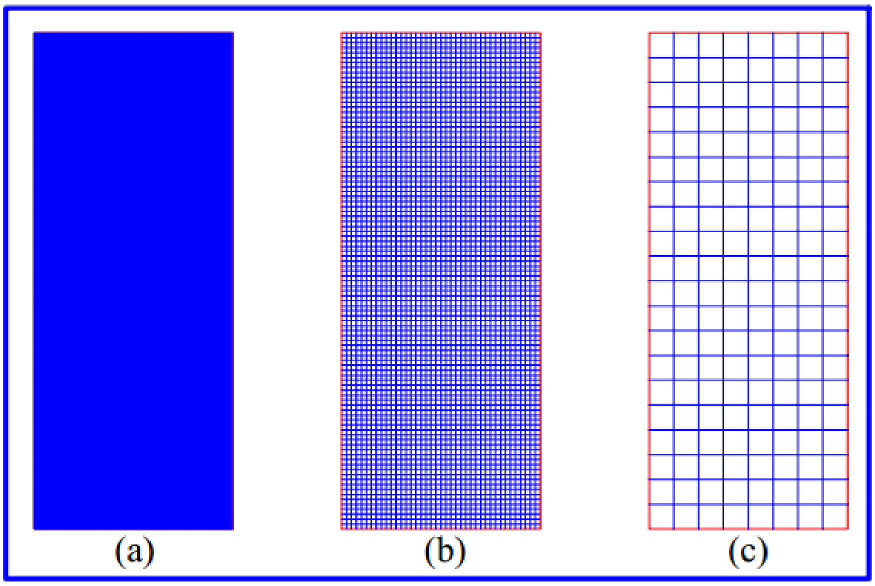

Fig. 4 The numerical grids of three schemes

Table 1 Comparison of different grid quantities on the outlet air temperature

	Grid quantity	Average temperature of air at outlet/K	Relative change/%(relative to the former scheme)
Scheme1	40000	1070.141	/
Scheme2	4000	1068.096	0.19
Scheme3	160	1030.944	3.48

The relative change of Scheme 2 is less than 2% compared to Scheme 1 as it is clearly shown in Table1. To obtain the accurate result with consider the consuming time a domain grid of Scheme 2 is adopted. Furthermore, the minimum convergence criterion for the velocity and continuity equation is 10^{-6} and for energy equation is 10^{-8}.

4.4 Boundary conditions

At the inlet, the velocity boundary condition is specified for the gas phase with no solid flow. Initially, solid particle velocity is set at zero. Air is uniformly applied at the bottom of the bed. At the outlet of the bed, the atmospheric boundary condition is employed. In gas-solid heat transfer process, wall boundary conditions for the solid phase can be defined in several ways such as no-slip, free-slip and partial-slip conditions [58]. In the actual investigations, the no-slip boundary condition applied to the gas phase at the walls, as it is important only in very dilute flows [59] . Moreover, the wall condition for the solid phase can also be set as no-slip by assuming that it has minor impact on the bed hydrodynamics. Nevertheless, the models with fine meshing, the impact of the wall boundary conditions might still be visible near the walls. To mitigate this issue, the partial-slip wall boundary condition model proposed by Ramzan *et al.* [60], which is applied here for the solid phase. This model uses a term 'specularity coefficient' to describe the wall frictional effects. Herein, a value of 0.1 is used for the specularity coefficient. The investigated parameters are summarized in Table 2.

Table 2 Simulation parameters

Gas property	
Density	1.225 kg/m^3
Viscosity	1.789×10^{-5} Pa·s
Temperature	300 K
Specific heat capacity	1006.430 J/(kg • K)
Thermal conductivity	0.024 W/(m • K)
superficial gas velocity	0.3,0.5,0.7,0.9 m/s

Atmosphere pressure	1.01×10^5 Pa
Solid property	
Diameter	0.02-0.1 m
Density	2500 kg/m^3
Temperature	1123 K
Specific heat capacity	920 J/(kg • K)
Thermal conductivity	0.230 W/(m • K)

In this study, the initial values of the variables for all the fields are specified for the entire computational domain. The walls boundary conditions for the energy equation are set as adiabatic, and that means the heat flux is thoroughly transferred from particles to air. The temperature (T_α) and viscosity (μ_α) of the cool air is taken as 300 K and 1.789×10^{-5} Pa·s, respectively, while the activation temperature (T_s) of CFA is 1123 K. All investigations are performed for a total time of 3-5 s with a time step of 0.01 s.

5. Results and discussion

5.1 Effect of solid diameter on the outlet air temperature

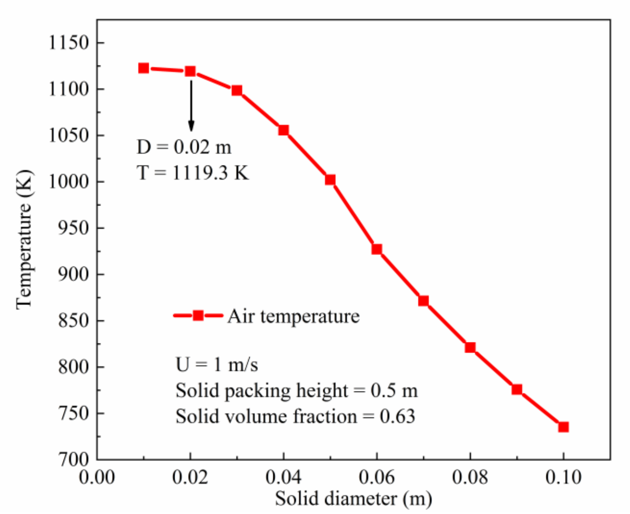

Fig. 5 Effect of solid diameter on the outlet air temperature of the bed

Investigations are carried out to analyze the effect of the particle size D on outlet air temperature in packed bed at the following design or operating conditions: U is supposed as 1 m/s, solid packing height is assumed as 0.5 m and solid volume fraction is set as 0.63 and they are validated in next section. The cost of pulverization in connection with solid diameter needs to be considered resulting from the agglomeration of CFA. Thereby, in order to determine suitable particle diameter, it is critical to establish a balance between the outlet air temperature of bed and solid diameter. The air temperature has a nearly linear decrease with the particle diameter vary 0.02 m to 0.1 m as described in Fig. 5. Obviously the surface area of particles grows with the decreasing diameter of particles, which results in the increase of convective heat transfer rate. Accordingly, the outlet air temperature reduces with the grow size of the particle. In addition, it is evident that the temperature difference is less for different size particles of smaller than 0.03 m.

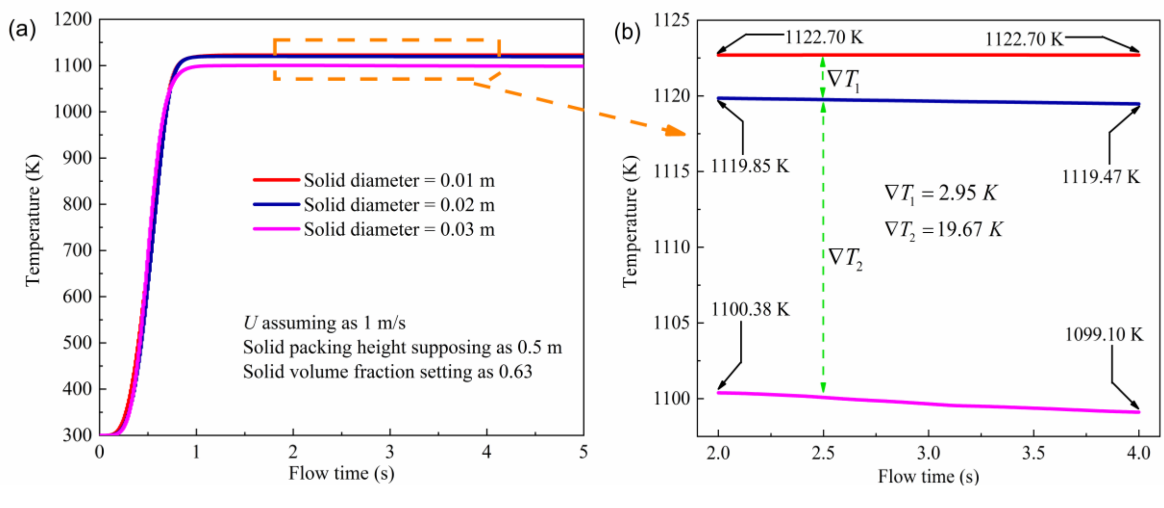

Fig. 6 The outlet air temperature of the bed with the solid diameter 0.01 m, 0.02 m and 0.03 m

The comparisons of outlet air temperature for different particle diameter within five seconds are demonstrated in Fig. 6a. The relative change of size 0.02 m is 2.95 K compared to size 0.01 m and 19.67 K compared to size 0.03 m. The Fig. 6b describes the variation of outlet air temperature at two to four seconds. The presented results show that the outlet air temperature decreases over time, while the larger particle size, the outlet air temperature decreases more quickly. The reason behind this phenomenon is that the heat recovery process of packed bed operates intermittently. The heat is continuously carried away from a certain amount of activated CFA via moving air. Another reason is that the inner heat of the solid needs to be conducted on the solid surface due to the larger size of particles. Considering the cost of activated CFA pulverization and outlet air temperature, a value of D of 0.02 m as usual is employed to ensure higher outlet air temperature of 1119.3 K.

5.2 Effect of superficial air velocity (U) on the outlet air temperature

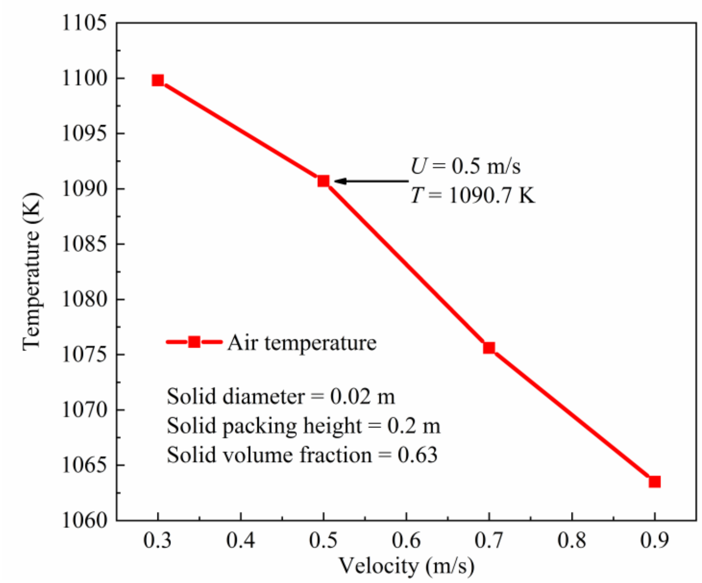

Fig. 7 Effect of superficial air velocity on the outlet air temperature of the bed

The convective heat transfer of two phases can be impacted by superficial air velocity. To investigate the effect of inlet cool air velocity on gas-solid heat transfer in the packed bed, airflow is varied with the help of valves. The influence of the superficial air velocity, U, is analyzed based on outlet air temperature under constant operating conditions for D is 0.03m, solid packing height assuming as 0.2 m, solid volume fraction supposing as 0.63. Afterwards, the effect of inlet air velocity on the outlet air temperature is given in Fig. 7, plotted for the velocity of 0.3 m/s, 0.5 m/s, 0.7 m/s and 0.9 m/s respectively. It is interesting to see that the temperature is nearly robotically perfect linear reduce vary 0.3 m/s to 0.9 m/s. It can be generally stated that the gas-solid contact time decreases by increasing the superficial air velocity, which results in the reduction in the heat transfer rate. Meanwhile, the increase of the superficial air velocity will raises the energy cost associated with air blowers. Compared with the particle diameter, inlet air velocity does not have evident influences on the outlet air temperature. Furthermore, to reduce the energy cost of air blowers, low inlet air velocity is applied for our investigation condition.

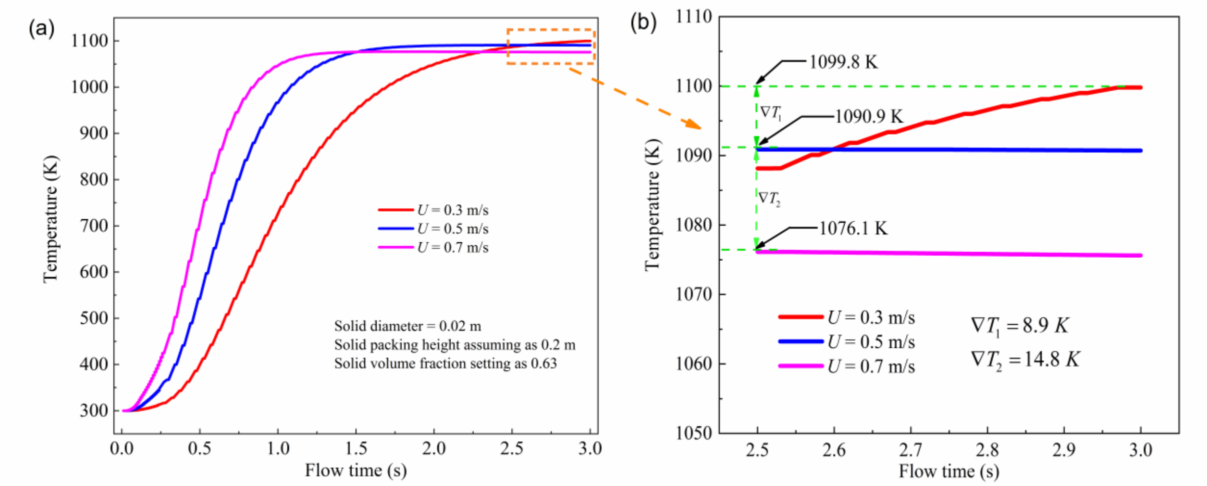

Fig. 8 The outlet air temperature of the bed with superficial air velocity 0.3 m/s, 0.5 m/s and 0.7 m/s

Comparisons of U at 0.3 m/s, 0.5 m/s and 0.7 m/s for outlet air temperature with three seconds are described in Fig. 8a. It is found that low superficial air velocity requires more time to get the hot air with a higher temperature, while the fast superficial air velocity requires less time to get the hot air with no much different temperature. Fig. 8b illustrates the variation of outlet air temperature at two point five seconds to three seconds. Such values reveal that the relative change of U at 0.5 m/s is 8.9 K compared to U at 0.3 m/s and 14.8 K in comparison with U at 0.7 m/s, which suggest that the effect of superficial air velocity tends to be increased. Generally, the higher air velocity leads to an improvement in the mixing properties to promote heat transfer rate but a reduction of two phases heat transfer contact time, as such the outlet air temperature decrease slightly. A value of U at 0.5 m/s is typically employed to attain the hot air with the temperature is 1090.7 K. In view of energy cost associated with air blowers and outlet air temperature, therefore U at 0.5m/s is selected as our operation conditions.

5.3 Effect of solid packing height on the outlet air temperature

The effect of the solid packing height on the outlet air temperature is investigated under following design or operating conditions of D at 0.02 m, U at 0.5 m/s and solid volume fraction assuming as 0.63. In this work, activated CFA is filled in the bed with the different height. The packing height of the bed strongly affects the contact time of two phases with the constant inlet superficial air velocity. The influence of solid packing height in the bed on outlet air temperature is demonstrated in Fig. 9, plotted for the packing height from 0.1 m to 0.9 m at intervals of 0.1 m. It is obvious that the outlet air temperature increases by increasing the solid particle packing height. However, the outlet air temperature exist no significant difference when the packing height exceeds 0.3 m. The reason is that the gas-solid temperature difference is negligible resulting from thermal balance between solid and air in the upper zone of packing area. Accordingly, more cool air is needed to extract heat from the solid at higher solid particle packing height. Hence, for obtaining enough hot air and saving the operation cost, the lower solid packing height is more favorable for our research.

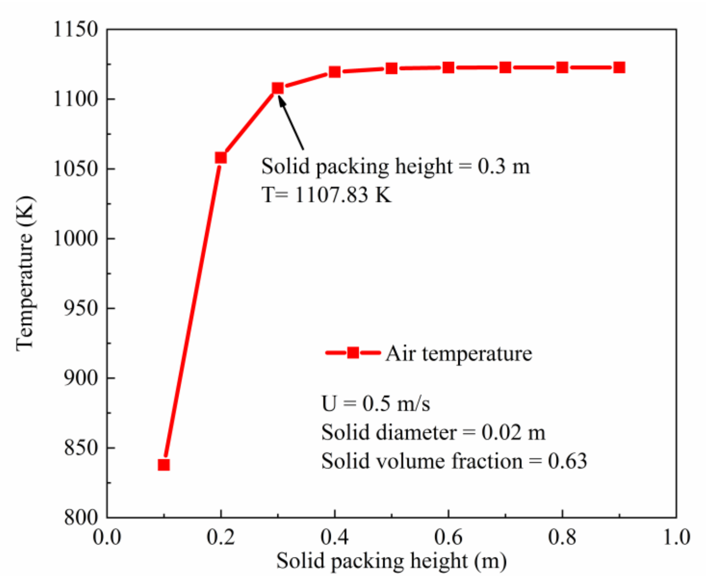

Fig. 9 Effect of solid packing height on the outlet air temperature of the bed

Fig. 10a illustrates comparisons of solid packing height at 0.2 m, 0.3 m and 0.4 m for outlet air temperature with the flow time at five seconds. The process of waste heat recovery requires same time to attain similarly temperature of air when the solid packing height is 0.3 m and 0.4 m respectively. In contrast, it will require a longer time to get the lower temperature of the air when the solid packing height is 0.2 m. Fig. 10b depicts the variation of outlet air temperature at 2.5 seconds to 4 seconds. Compared with the solid packing height of 0.3 m, the relative temperature difference is 0.8 K at solid packing height of 0.4 m and 40.8 K at solid packing height of 0.2 m, which illustrates that the effect of solid packing height tends to increase. The higher solid particle packing height results in an improvement of two phases contact time to promote heat transfer rate, however, the convective heat transfer remarkably declines owing to the decrease of temperature difference between air and solid in the upper zone of the bed when the packing height exceeds 0.3 m. A value of solid particle packing height of 0.3 m is typically employed to obtain the hot air with the temperature of 1108.9 K. In order to achieve the longer time of a single batch operation and get the higher outlet air temperature, solid particle packing height of 0.3 m is considered as minimize packing height.

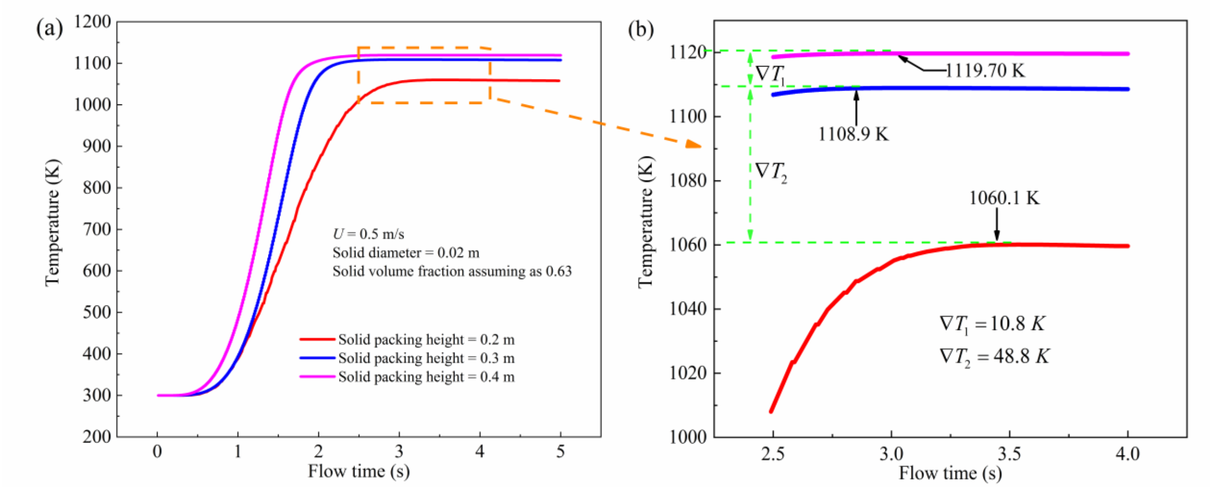

Fig.10. The outlet air temperature of the bed with solid packing height 0.2 m, 0.3 m and 0.4 m

5.4 Effect of solid volume fraction on the outlet air temperature

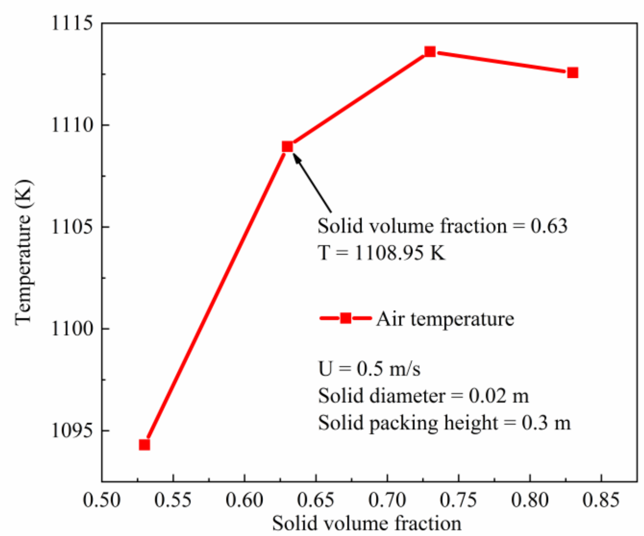

Fig.11. Effect of solid volume fraction on the outlet air temperature of the bed

The influence of solid particle volume fraction is analyzed in view of the outlet air temperature for constant operating conditions of D at 0.02 m, U at 0.5 m/s, solid particle packing height at 0.3 m. Activated CFA is filled in the bed with the packing height of 0.5 m. The four solid volume fractions are selected for this comparison, which is 0.53, 0.63, 0.73 and 0.83 respectively. As is evident in Fig. 11, the outlet air temperature grows with the solid particle volume fraction owing to the reducing porosity of the packed bed, which enhances convective heat transfer between air and particle surface. However, the trend of increase has slowed down when the volume fraction exceeds 0.63. Small porosity of the packed bed will increase the velocity of the air passing through the packing area. Thereby, the reduction of gas-solid contact time results in the lower convective heat transfer rate. Meanwhile, airflow resistance grows with the increase of the solid packing volume fraction, which gives rise to the increase of the energy cost associated with air blowers. We found out that the lower solid packing volume fraction is more suitable to reduce the energy cost of air blowers.

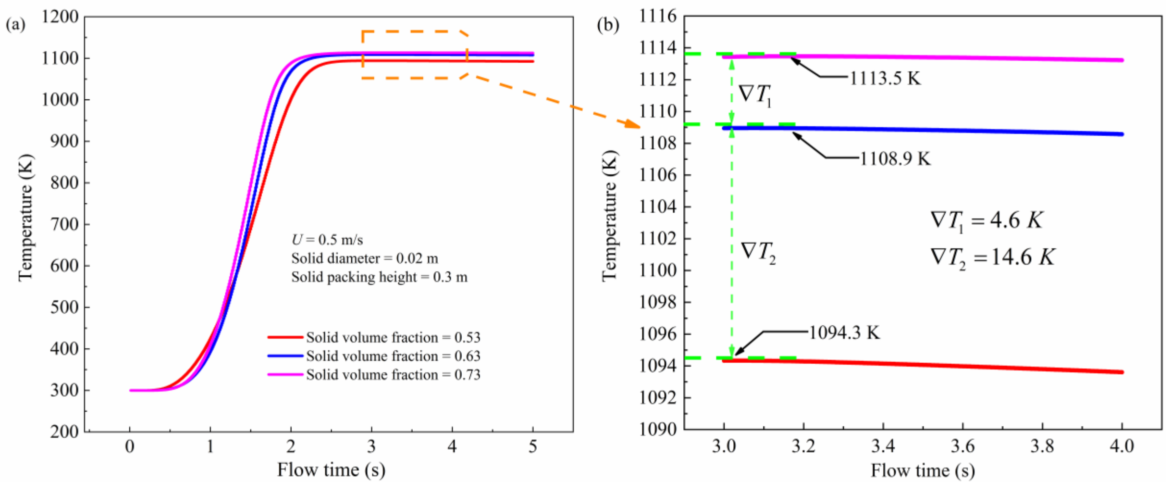

Fig. 12 The outlet air temperature of the bed with solid volume fraction 0.53 m, 0.63 m and 0.73 m

Comparisons of solid packing volume fraction at 0.53 m, 0.63 m and 0.73 m for outlet air temperature with five seconds are demonstrated in Fig. 12a. There is no significant difference in outlet air temperature for three investigated cases. The variation of outlet air temperature at three to four seconds is depicted in Fig. 12b. Compared with the solid packing volume fraction of 0.63, the relative temperature difference is 4.6 K at solid packing volume fraction of 0.73 and 14.6 K with solid packing volume fraction of 0.53, which demonstrates that the solid packing volume fraction does not have significant influence on the outlet air temperature. When the solid packing height exceeds 0.3 m, gas-solid two phases can also achieve thermal balance state in the upper zone of the packed bed with different volume fraction. Moreover, the porosity of packing zone becomes the key factor affecting the outlet air temperature. Hence, the process of waste heat recovery requires less time to obtain the air with nearly same temperature for the larger packing volume fraction. The corresponding airflow resistance also rises with the solid packing volume fraction. A value of solid particle packing volume fraction of 0.63 is applied to obtain the hot air with the temperature at 1108.9 K. For reducing airflow resistance and rising outlet air temperature, as such solid particle packing volume fraction of 0.63 is applied for our investigation case.

5.5 The air temperature distribution in the bed

Prior to building a packed bed for heat recovery from activation CFA, it is critical to know the characteristic of packing zone needed to reach thermal steady state condition. Activation CFA is filled in the bed at 1123 K. Fig. 13 describes air temperature distribution at time instant of 0.5, 1.0, 1.5 and 2.0s. The investigation parameters is set as *D* at 0.02 m, *U* at 0.5 m/s, solid packing height at 0.5 m and solid volume fraction at 0.63.

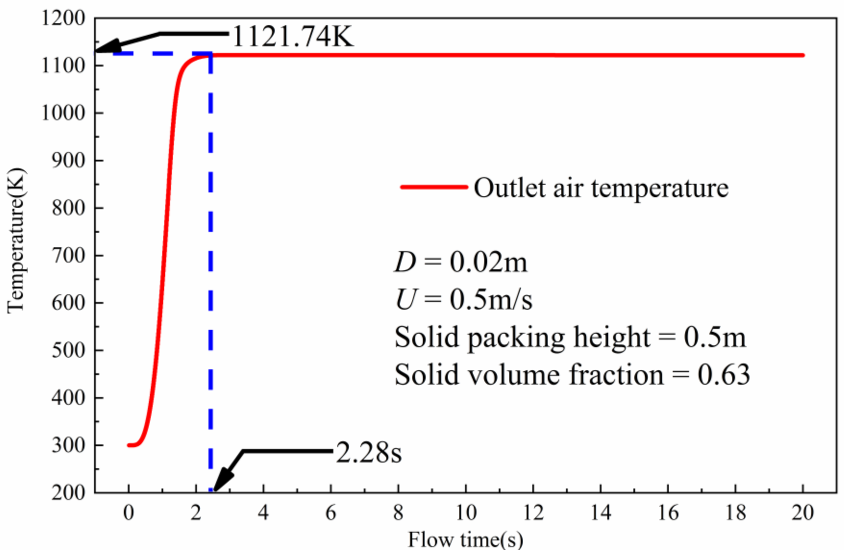

Fig. 13 Outlet air temperature profiles with flow time for D= 0.02 m, U=0.5 m/s, Solid packing height=0.5 m, Solid volume fraction=0.63

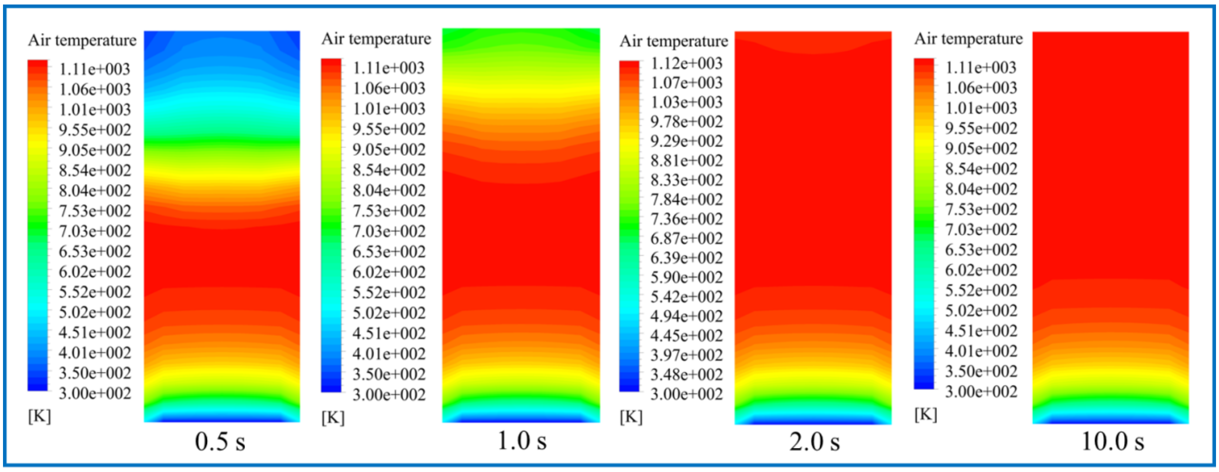

Fig. 14 Snapshots of air temperature at different times for the simulation case (*D*=0.02 m, *U*=0.5 m/s, Solid packing height=0.5 m, Solid volume fraction=0.63)

The gas-solid flow is complex and heterogamous due to intense air turbulence, drastic gas-solid momentum exchange, and interphase heat transfer in the packing zone, especially the lower part. Cold air is introduced to the bed from the bottom distributor and valve. Accordingly, of note is that the two-phase convection heat transfer is ongoing with insufficient contact time for the gas-solid in the lower section of the bed result in the air temperature has a low value. In the meanwhile, the larger temperature difference between two-phase enhances convective heat transfer rate. As depicted in Fig. 14, the air has a higher temperature near the wall at the same horizontal of the packing zone. Actually, due to the viscosity of the fluid and the wall interface blocking, the air velocity near the wall will be blocked and slow down. The intensified interphase heat transfer results from the longer two-phase contact time near the wall. From the temperature clouds illustrated in Fig. 14, the process of waste heat recovery achieving steady thermal balance state in the upper zone of bed after two seconds. It also can be found that temperature increases significantly with the bed height and the outlet air temperature is 1121.74 K. Such value reveals that the packed bed is characterized by a short time to obtain enough hot air. Moreover, after two seconds, the hot air exist no temperature gradients at the outlet of the packed bed.

6. Conclusions

In this study, unsteady behavior of waste heat recovery from activated CFA has been investigated based on Euler-Euler modeling incorporating the kinetic theory of phase flow. The energy transport in packed bed can be described through solving energy conversion differential equations in two phases. The air temperature field among packed particles is resolved by considering the radial in homogeneous distribution of porosity and the effective fluid viscosity. The influence of several key design and operating variables on the outlet air temperature of the packed bed are assessed, such as solid particle diameter, superficial air velocity, solid packing height and solid packing volume fraction.

The heat transfer characteristics of gas-solid phases and air temperature fields of the packed bed under some key conditions have been obtained successfully. The results revealed that the particle diameter strongly affect the heat transfer, as a smaller diameter particle with larger surface area yielded higher heat transfer to the fluid. By changing the packing height of the activated CFA in the bed, the outlet air temperature can be effectively improved. Meanwhile, the heat transfer ability between the gas and solid is utilized in the greatest extent when the packing height is 0.3 m. Afterwards, it is found that it has no enough time to achieve thermal equilibrium the between gas and solid at the higher air velocity, which results in the lower outlet air temperature. The investigation confirms that the solid volume fraction taken as 0.63 is favorable to heat recovery, which makes a compromise between the airflow resistance and outlet air temperature. The obtained distribution mechanism of the temperature field for gas phase based on the transient temperature contours at different times suggesting that the transfer of heat will continue as long as there is a difference in temperature between the two locations. Once the two locations have reached the same temperature, thermal equilibrium is established and the heat transfer will stop. As a result, the hot air exist no temperature gradients at the outlet of the packed bed. In addition, the insights emanating from the current work are worthwhile for the exploitation of technology of energy recovery from solid and design of such apparatuses in industrial fields. Nevertheless, the impact of outlet hot air on pre-heated raw CFA and energy recovery efficiency need further investigation in future work.

Acknowledgment

We greatly acknowledge the financial support provided by the National Key Research and Development Program (No.2017YFB0603105).

Nomenclature

Λ	mean free path of gas
Λ_0	mean free path of gas under 1 atm and 273.15 K
α_α	air volume fraction
α_s	solid volume fraction
$\alpha_{s,max}$	maximum solid volume fraction
α_T	thermal accommodation coefficient
β	interphase momentum transfer coefficient
C_p	thermal capacity of gas
d_p	particle diameter
E	Young's modulus
E'	effective elastic modulus
e	coefficient of restitution
F	normal contact force
F_i	the drag force between gas and solid
$\boldsymbol{g}$	gravity vector
g_0	radial distribution function
H^*	the mean micro hardness of particles
H_{bed}	the height of packing, m
h	convective heat transfer coefficient air-solid phase
$\boldsymbol{I}$	identity tensor
I_{2D}	second invariant of deviatoric stress tensor

κ_α air thermal conductivity

κ_s fly ash thermal conductivity

M gas parameter

M_α molecular mass of gas

M_s molecular mass of solid

m mean absolute surface slope

N_u nusselt number

P_α pressure of gas

P_s pressure of fly ash

P_r air Prandtl number

ρ_α air density

ρ_s fly ash density

Q power

$\mathrm{R}e$ Reynolds number

R_{ep} fly ash Reynolds number

R_j joint thermal resistance

R_S the micro-contact constriction/spreading resistance

R_L the macro-contact constriction/spreading resistance

R_G the resistance of interstitial gas in the macro-gap

R_g the resistance of interstitial gas in the micro-gap

r_L radius of macro-contact

r_H radius of Hertzian contact

γ collisional dissipation of solid fluctuating kinetic energy

T_s temperature of solid or particles

$\boldsymbol{u_\alpha}$ air velocity vector

$\boldsymbol{u_s}$ fly ash velocity vector

μ_α air viscosity

μ_s fly ash viscosity

σ mean surface roughness height

σ_s solid stress tensor

ζ_s fly ash bulk viscosity

θ granular temperature

ϕ internal friction angle

ψ non-dimensional parameter

η non-dimensional parameter

τ non-dimensional parameter

S non-dimensional parameter

B non-dimensional parameter

v Poisson's ratio

Γ ratio of gas specific heats

ε the voidage of the packed bed

k_α turbulence kinetic energy of gas phase

ε_α turbulent energy dissipation rate of gas phase

$\mu_{t,\alpha}$ gas phase turbulent viscosity

$G_{k,\alpha}$ rate of production of turbulent kinetic energy

$\Pi_{k,\alpha}$ turbulent interaction parameters

h_k interfacial tension of turbulence kinetic energy

h_ε interfacial tension of turbulent energy dissipation rate

References

[1] G. Kazas, E. Fabrizio, M. Perino, Energy demand profile generation with detailed time resolution at an urban district scale: A reference building approach and case study, *Appl. Energy*. 193 (2017) 243-262.

[2] Y. Huang, J. Zhang, Q. Zhang, S. Nie, Backfilling technology of substituting waste and fly ash for coal underground in china coal mining area, *Environ. Eng. Manage. J.* 10 (2011) 769-775.

[3] P.S. Varbanov, T.G. Walmsley, Y.V. Fan, J.J. Klemeš, S.J. Perry, Spatial targeting evaluation of energy and environmental performance of waste-to-energy processing, *Front. Chem. Sci. Eng.* 12 (2018) 731-744.

[4] T. Ferdan, M. Pavlas, V. Nevrlý, R. Šomplák, P. Stehlík, Greenhouse gas emissions from thermal treatment of non-recyclable municipal waste, *Front. Chem. Sci. Eng*. 12 (2018) 815-831.

[5] S. Kakarantzas, L.T. Benos, I. Sarris, B. Knaepen, A. Grecos, N. Vlachos, MHD liquid metal flow and heat transfer between vertical coaxial cylinders under horizontal magnetic field, *Int. J. Heat Fluid Flow*. 65 (2017) 342-351.

[6] Q. An, Y. Wang, J. Zhao, L. Chao, W. Yan, Direct utilization status and power generation potential of low-medium temperature hydrothermal geothermal resources in Tianjin, China: A

review, *Geothermics*. 64 (2016) 426-438.

[7] Huang, Hongna, Wang, Jinli, Zhang, Xiaoqiang, Optimal design of heat exchanger header for coal gasification in supercritical water through CFD simulations, *Chin. J. Chem. Eng.* 25 (2017) 1101-1108.

[8] J. Gao, C. Li, W. Liu, J. Hu, W. Lin, L. Qiang, B. Liang, H. Yue, G. Zhang, D. Luo, Process simulation and energy integration in the mineral carbonation of blast furnace slag, *Chin. J. Chem. Eng.* 27 (2018) 157-167.

[9] Z.T. Yao, X.S. Ji, P.K. Sarker, J.H. Tang, L.Q. Ge, M.S. Xia, Y.Q. Xi, A comprehensive review on the applications of coal fly ash, *Earth-Sci. Rev.* 141 (2015) 105-121.

[10] Y. Wu, X. Ping, C. Jiao, L. Li, M. Li, Effect of Temperature on Phase and Alumina Extraction Efficiency of the Product from Sintering Coal Fly Ash with Ammonium Sulfate, *Chin. J. Chem. Eng.* 22 (2014) 1363-1367.

[11] F. Cheng, L. Cui, J.D. Miller, X. Wang, Aluminum leaching from calcined coal waste using hydrochloric acid solution, *Miner. Process. Extr. Metall. Rev.* 33 (2012) 391-403.

[12] C. Guo, Z. Shen, Q. Hu, S. Wang, F. Ling, The solvothermal synthesis, structure and properties of $Al_2O_3 \cdot TiO_2$ mesoporous material, *Mater. Chem. Phys.* 151 (2015) 288-294.

[13] B. Zhou, J. Zhou, T. Hu, L. Yang, G. Lin, L. Zhang, Phase transformation mechanism in activation of high-alumina fly ash with Na_2CO_3, *Mater. Res. Express.* 6 (2018) 015502.

[14] X.W. Yao, K.L. Xu, Y. Li, Experimental investigation of performance properties and agglomeration behavior of fly ash from gasification of corncobs, *J Cent South Univ.* 24 (2017) 496-505.

[15] J.J. Cai, J.J. Wang, C.X. Chen, L.U. Zhong-Wu, Recovery of residual-heat integrated

steelworks, *Iron & Steel.* 42 (2007) 1-7.

[16] Y. Ding, D.M. Shi, High-efficiency utilization of waste heat at fully integrated steel plant, *Iron & Steel.* 46 (2011) 88-98.

[17] Y. Chen, Numerical simulation study on waste heat recovery system of high temperature steel slag, *Shandong Univ.* (2014).

[18] T. Atmakidis, E.Y. Kenig, Numerical analysis of mass transfer in packed-bed reactors with irregular particle arrangements, *Chem. Eng. Sci.* 81 (2012) 77-83.

[19] R. Sundaresan, A.K. Kolar, Axial heat transfer correlations in a circulating fluidized bed riser, *Appl. Therm. Eng.* 50 (2013) 985-996.

[20] H. Yoshida, K. Fukui, K. Yoshida, E. Shinoda, Particle separation by Iinoya's type gas cyclone, *Powder Technol.* 118 (2001) 16-23.

[21] B.G. García, G.S. Grasa, M.A. Carreño, J.C.A. García, Modeling of the Deactivation of CaO in a Carbonate Loop at High Temperatures of Calcination, *Ind. Eng. Chem. Res.* 47 (2008) 9256-9262.

[22] Shengfu, Chengyue, Intensification of Deep Hydrodesulfurization Through a Two-stage Combination of Monolith and Trickle Bed Reactors, *Chin. J. Chem. Eng.* 22 (2014) 888-897.

[23] C. Dai, F. Gu, Thermophoresis effects on gas-particle phases flow behaviors in entrained flow coal gasifier using Eulerian model, *Chin. J. Chem. Eng.* 25 (2017) 712-721.

[24] G. Karthik, V.V. Buwa, Effect of particle shape on fluid flow and heat transfer for methane steam reforming reactions in a packed bed, *AIChE J.* 63 (2017) 366-377.

[25] B. Hou, R. Ye, Y. Huang, X. Wang, Z. Tao, A CFD model for predicting the heat transfer in the industrial scale packed bed, *Chin. J. Chem. Eng.* 26 (2018) 228-237.

[26] M. Nijemeisland, A.G. Dixon, CFD study of fluid flow and wall heat transfer in a fixed bed of spheres, *AIChE J.* 50 (2010) 906-921.

[27] A. Guardo, M. Coussirat, M.A. Larrayoz, F. Recasens, E. Egusquiza, Influence of the turbulence model in CFD modeling of wall-to-fluid heat transfer in packed beds, *Chem. Eng. Sci.* 60 (2005) 1733-1742.

[28] N. Zobel, F. Behrendt, Transient heat transfer in packed beds: The significance of the history term, *Int. J. Heat Mass Transfer.* 51 (2008) 3816-3824.

[29] H.P. Zhu, Z.Y. Zhou, R.Y. Yang, A.B. Yu, Discrete particle simulation of particulate systems: Theoretical developments, *Chem. Eng. Sci.* 63 (2007) 5728-5770.

[30] F. Bambauer, S. Wirtz, V. Scherer, H. Bartusch, Transient DEM-CFD simulation of solid and fluid flow in a three dimensional blast furnace model, *Powder Technol.* 334 (2018) 53-64.

[31] J. Ding, D. Gidaspow, Bubbling fluidization model using kinetic theory of granular flow, *AIChE J.* 36 (2010) 523-538.

[32] Y.Q. Feng, A.B. Yu, Microdynamic modelling and analysis of the mixing and segregation of binary mixtures of particles in gas fluidization, *Chem. Eng. Sci.* 62 (2007) 256-268.

[33] S. Vun, J. Naser, P. Witt, Extension of the kinetic theory of granular flow to include dense quasi-static stresses, *Powder Technol*. 204 (2010) 11-20.

[34] S. Benyahia, M. Syamlal, T.J. O'Brien, Study of the ability of multiphase continuum models to predict core‐annulus flow, *AIChE J.* 53 (2007) 2549-2568.

[35] M. Hassan, M. Philip, M. Rafique, Y. Feng, G. Liu, P.J. Witt, S. Wang, H. Lu, Numerical simulations of solid circulation characteristics in an internally circulating elevated fluidized bed, *Chem. Eng. Technol.* 40 (2016) 769-777.

[36] H. Chen, S. Gu, H. Li, Simulation gas-solid flow in the downer with new structure-based drag model, *Powder Technol.* 323 (2018) 163-175.

[37] W. Du, X. Bao, J. Xu, W. Wei, Computational fluid dynamics (CFD) modeling of spouted bed: Assessment of drag coefficient correlations, *Chem. Eng. Sci.* 61 (2006) 1401-1420.

[38] D. Kunii, O. Levenspiel, H. Brenner, *Fluidization Engineering (Second Edition)*. (1991).

[39] D. W. Green, R. H. Perry, Perry's Chemical Engineers' Handbook, *Perry*. (1997).

[40] M. Bahrami, M.M. Yovanovich, J.R. Culham, Effective thermal conductivity of rough spherical packed beds, *Int. J. Heat Mass Transfer.* 49 (2006) 3691-3701.

[41] W.V. Antwerpen, P.G. Rousseau, C.G.D. Toit, Multi-sphere Unit Cell model to calculate the effective thermal conductivity in packed pebble beds of mono-sized spheres, *Nucl. Eng. Des.* 247 (2012) 183-201.

[42] X. Wang, J. Zheng, H. Chen, A prediction model for the effective thermal conductivity of mono-sized pebble beds, *Fusion Eng. Des.* 103 (2016) 136-151.

[43] O. Bey, G. Eigenberger, Gas flow and heat transfer through catalyst filled tubes, *Int. J. Therm. Sci.* 40 (2001) 152-164.

[44] W. Ranz, W.R. Marshall, Evaporation from drops, *Chem. eng. prog*. 48 (1952) 141-146.

[45] J. Soria, D. Gauthier, G. Flamant, R. Rodriguez, G. Mazza, Coupling scales for modelling heavy metal vaporization from municipal solid waste incineration in a fluid bed by CFD, *Waste Manag*. 43 (2015) 176-187.

[46] X. Chen, P. Han, A note on the solution of conjugate heat transfer problems using SIMPLE-like algorithms, *Int. J. Heat Fluid Flow.* 21 (2000) 463-467.

[47] D. Gidaspow, Multiphase flow and fluidization: Continuum & Kinetic Theory Description, *Academic press*. (1994) 1-29.

[48] F. Vejahati, N. Mahinpey, N. Ellis, M.B. Nikoo, CFD simulation of gas-solid bubbling fluidized bed: A new method for adjusting drag law, *Can. J. Chem. Eng.* 87 (2009) 19-30.

[49] M.J.V. Goldschmidt, J.A.M. Kuipers, W.P.M.V. Swaaij, Hydrodynamic modelling of dense gas-fluidised beds using the kinetic theory of granular flow: effect of coefficient of restitution on bed dynamics, *Chem. Eng. Sci.* 56 (2001) 571-578.

[50] S. Wang, X. Li, H. Lu, L. Yu, D. Sun, Y. He, Y. Ding, Numerical simulations of flow behavior of gas and particles in spouted beds using frictional-kinetic stresses model, *Powder Technol.* 196 (2009) 184-193.

[51] H. Lu, Y. He, D. Gidaspow, L. Yang, Y. Qin, Size segregation of binary mixture of solids in bubbling fluidized beds, *Powder Technol.* 134 (2003) 86-97.

[52] M.F. Rahaman, J. Naser, P.J. Witt, An unequal granular temperature kinetic theory: description of granular flow with multiple particle classes, *Powder Technol*. 138 (2003) 82-92.

[53] H.P. Zhu, Z.Y. Zhou, A.B. Yu, P. Zulli, Stress fields of solid flow in a model blast furnace, *Granular Matter.* 11 (2009) 269-280.

[54] H.P. Zhu, Q.F. Hou, Z.Y. Zhou, A.B. Yu, Averaging method of particulate systems and its application to particle-fluid flow in a fluidized bed, *Chin. Sci. Bull.* 54 (2009) 4309-4317.

[55] O. Derkx, A. Dixon, Determination of the fixed bed wall heat transfer coefficient using computational fluid dynamics, *Numer. Heat Transfer.* 29 (1996) 777-794.

[56] G. Hindi, E. Paladino, A. de Oliviera, Effect of mesh refinement and model parameters

on LES simulation of diesel sprays, *Int. J. Heat Fluid Flow.* 71 (2018) 246-259.

[57] R. Mckelvey, A. Mclennan, T. Turocy, Gambit: Software Tools for Game Theory, *Mod. Hosp.* 41 (2006).

[58] M. Yoon, J. Hwang, J. Lee, H.J. Sung, J. Kim, Large-scale motions in a turbulent channel flow with the slip boundary condition, *Int. J. Heat Fluid Flow.* 61 (2016) 96-107.

[59] P. Fede, O. Simonin, A. Ingram, 3D numerical simulation of a lab-scale pressurized dense fluidized bed focussing on the effect of the particle-particle restitution coefficient and particle-wall boundary conditions, *Chem. Eng. Sci.* 142 (2016) 215-235.

[60] M. Ramzan, M. Farooq, T. Hayat, J.D. Chung, Radiative and Joule heating effects in the MHD flow of a micropolar fluid with partial slip and convective boundary condition, *J. Mol. Liq.* 221 (2016) 394-400.